Advances in Difference Equations
a SpringerOpen Journal

RESEARCH

Open Access

Bifurcation analysis of a two-dimensional discrete Hindmarsh–Rose type model

Bo Li[1]* and Qizhi He[1]

*Correspondence: libo@aufe.edu.cn; libomaths@163.com
[1]School of Finance, Anhui University of Finance and Economics, Bengbu, People's Republic of China

Abstract

In this paper, bifurcation analysis of a discrete Hindmarsh–Rose model is carried out in the plane. This paper shows that the model undergoes a flip bifurcation, a Neimark–Sacker bifurcation, and 1 : 2 resonance which includes a pitchfork bifurcation, a Neimark–Sacker bifurcation, and a heteroclinic bifurcation. The sufficient conditions of existence of the fixed points and their stability are first derived. The flip bifurcation and Neimark–Sacker bifurcation are analyzed by using the inner product method and normal form theory. The conditions for the occurrence of 1 : 2 resonance are also presented. Furthermore, the sufficient conditions of pitchfork, Neimark–Sacker, and heteroclinic bifurcations are derived and expressed by implicit functions. The numerical analysis shows us consistence with the theoretical results and exhibits interesting dynamics, especially symmetric and invariant closed orbits. The dynamics observed in this paper can be used to mimic the dynamical behaviors of one single neuron and design a humanoid locomotion model for applications in bio-engineering and so on.

MSC: 37G05; 37G35; 39A10

Keywords: Hindmarsh–Rose model; Flip bifurcation; Pitchfork bifurcation; Neimark–Sacker bifurcation; 1 : 2 resonance; Symmetric orbits

1 Introduction

In 1952, Hodgkin and Huxley constructed the so-called Hodgkin–Huxley mathematical model to mimic the neural activities of the squid giant [1]. Despite the excellent ability in the description of neural activities, the model is so complex that many applied mathematicians and neuroscientists simplified the model through reducing the number of variables and constants. For one single neuron, FitzHugh [2] and Nagumo et al. [3] introduced the following simplified version of the Hodgkin–Huxley equations, which only contains two variables:

$$\begin{cases} \frac{dx}{dt} = \alpha(y - f(x) + I), \\ \frac{dy}{dt} = \beta(g(x) - y), \end{cases} \tag{1}$$

where x is the membrane potential, y is a recovery variable, and I is the stimulus intensity. Based on model (1), Hindmarsh and Rose [4, 5] introduced two- or three-dimensional neural models which provide a more realistic description of firing. To describe three fundamental activities of a single neuron, such as the quiescence, (irregular) spiking, and

(irregular) bursting, some different versions of Hindmarsh–Rose type model have been introduced from different viewpoints. The dynamical behaviors and the related applications have been investigated by many researchers from different academic backgrounds. Zhang et al. [6] discussed the key properties of Hindmarsh–Rose model and designed a new kind of central pattern generator, which can be used to construct a humanoid locomotion model and mimic the dynamics of a functional electrical walking system. Hindmarsh–Rose-like electronic oscillator was used to construct a capacitive microelectromechanical system by Domguia et al. [7], and the transfer of different electronic signal meant occurrence and transition between quiescence, spiking, and bursting oscillation. Furthermore, this can give us some insights into bio-engineering, such as artificial heart.

During the last ten years, many researchers have studied the complex dynamics of a Hindmarsh–Rose-type system with the help of bifurcation theory. Wu et al. [8] discussed the bifurcation pictures of a kind of the modified Hindmarsh–Rose model as one or two parameters vary. Period-adding bifurcation, period-doubling bifurcation, and intermittent chaotic phenomena were computed numerically and plotted to be observed clearly. When parameters vary, the bifurcation occurs and the behaviors of neurons are explained. Yu and Cao [9] presented the existence of one-parameter bifurcations of three-dimensional discrete Hindmarsh–Rose, and numerical simulations were given to illustrate the bifurcation analysis. One can find more information on bifurcations of the Hindmarsh–Rose-type model in [10–18] and on related one(two)-parameter bifurcation theory in [19–27]. Herein, we discuss the following revised model [28] in 2007:

$$\begin{cases} \frac{dx}{dt} = c(x - \frac{x^3}{3} - y + I), \\ \frac{dy}{dt} = \frac{x^2 + dx - by + a}{c}, \end{cases} \tag{2}$$

where parameters a, b, c, and d are positive. Numerical bifurcation studies for model (2) were presented along with physiological simulations. They discussed some bifurcation structures such as fold bifurcations for equilibria and limit cycle, Hopf bifurcations, cusp bifurcations, and Bogdanov–Takens bifurcations for equilibria. These results show the complex and interesting dynamics included in model (2). In [29], the author analyzed the stability of the equilibria and examined the bifurcation scenarios qualitatively. The existence and the critical normal form of Hopf bifurcation and two of its degenerate cases were computed, and numerical analysis for the conditions was provided to illustrate the theoretical results. Heidarpur et al. proposed a piecewise linear version of model (2) and the relations between them were analyzed by using digital implementation in [30]. Meanwhile, there has been an increasing interest in investigating the dynamics of discrete-time models [19–21, 23–25, 27].

We apply the Euler method to model (2) and obtain the following map:

$$\begin{pmatrix} x \\ y \end{pmatrix} \mapsto \begin{pmatrix} x + \delta c(x - \frac{x^3}{3} - y + I) \\ y - \frac{\delta}{c}(x^2 + dx - by + a) \end{pmatrix}, \tag{3}$$

where δ is a positive step size. In our paper, we use the inner product method to compute the critical normal form of two kinds of one-parameter bifurcations and the generate case, $1 : 2$ resonance, at fixed points of map (3).

The rest of this paper is presented as follows. In Sect. 2, the number and stability of fixed points for map (3) are computed. In Sect. 3, we provide sufficient conditions for flip bifurcation and Neimark–Sacker bifurcation at the fixed points of map (3). In Sect. 4, the step sizes δ and d are chosen as free parameters to explore the local dynamics induced by $1:2$ resonance, and we present the sufficient conditions for $1:2$ resonance at the fixed points of map (3). In Sect. 5, numerical analysis is provided to illustrate the theoretical results, and complex dynamics are observed, especially period-doubling phenomena, symmetric closed circle, and heteroclinic structure. Finally, conclusions are summarized in Sect. 6.

2 Existence and stability of fixed points of map (3)

The fixed points of map (3) satisfy the following equations:

$$
\begin{cases}
x - \frac{x^3}{3} - y + I = 0, \\
x^2 + dx - by + a = 0.
\end{cases}
\tag{4}
$$

After variable replacements, we get the following conditions for $E(x, y)$ as a fixed point of map (3):

$$
F(x) = \frac{b}{3}x^3 + x^2 + (d - b)x + a - bI = 0,
\tag{5}
$$

and

$$
y = x - \frac{x^3}{3} + I.
\tag{6}
$$

The effect of I is reflected through parameters a and b [28], and we suppose that $I = 0$ in this paper. Then equations (5) and (6) become

$$
F(x) = \frac{b}{3}x^3 + x^2 + (d - b)x + a = 0
\tag{7}
$$

and

$$
y = x - \frac{x^3}{3}.
$$

It is clear that $F(x)$ of equation (7) is a smooth function, and calculus on monotonicity is used to investigate the existence of solutions of (7). The following results can be got [29].

Lemma 2.1 *Define* $D = 1 + b^2 - bd$, $x_l = \frac{-1-\sqrt{D}}{b}$, *and* $x_r = \frac{-1+\sqrt{D}}{b}$, *then*:
  (i) *If* $D \leq 0$, *there exists a unique fixed point* $E_{11}(x_{11}^*, y_{11}^*)$ *for map* (3), *where* $x_{11}^* < 0$;
  (ii) *If* $D > 0$ *and* $F(x_l)F(x_r) > 0$, *there exists a unique fixed point* $E_{11}(x_{11}^*, y_{11}^*)$ *for map* (3), *where* $x_{11}^* < x_l < 0$ (*resp.,* $x_r < x_{11}^* < 0$) *when* $b \geq d$ (*resp.,* $b < d$);
  (iii) *If* $D > 0$ *and* $F(x_l)F(x_r) = 0$, *there exist two fixed points* $E_{21}(x_{21}^*, y_{21}^*)$ *and* $E_{22}(x_{22}^*, y_{22}^*)$ *for map* (3), *where* $x_{21}^* = x_l < x_r < x_{22}^* < 0$ (*resp.,* $x_{21}^* < x_l < 0 < x_{22}^* = x_r$) *when* $b \geq d$ (*resp.,* $b < d$);
  (iv) *If* $D > 0$ *and* $F(x_l)F(x_r) < 0$, *there exist three fixed points* $E_{31}(x_{31}^*, y_{31}^*)$, $E_{32}(x_{32}^*, y_{32}^*)$, *and* $E_{33}(x_{33}^*, y_{33}^*)$ *for map* (3), *where* $x_{31}^* < x_l < x_{32}^* < x_r < x_{33}^* < 0$ (*resp.,* $x_{31}^* < x_l < 0 < x_{32}^* < x_r < x_{33}^*$) *when* $b \geq d$ (*resp.,* $b < d$).

Figure 1 Solution curves in $(x, d, F(x))$ space
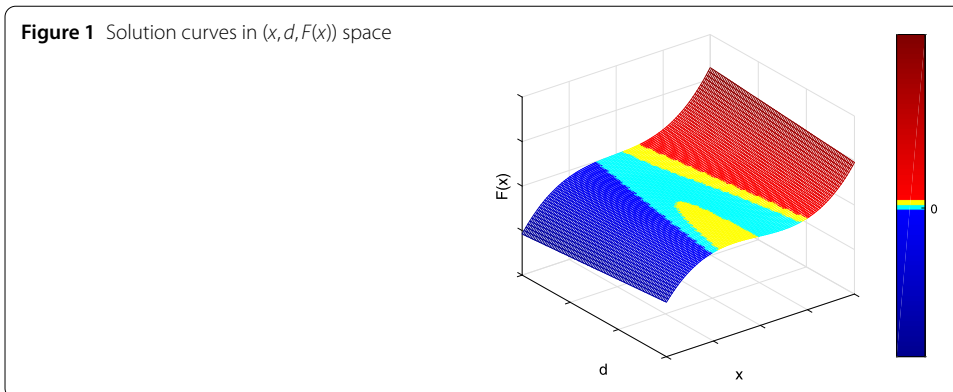
In Fig. 1, the distribution of solution is plotted in a three-dimensional space to illustrate the properties discussed in Lemma 2.1.

Now we construct the following Jacobian matrix to investigate the stability of the fixed point $E^*(x^*, y^*)$ of map (3), which can be denoted as one of the above six fixed points listed in Lemma 2.1:

$$A(\delta, d, x^*, y^*) = \begin{pmatrix} 1 + \delta c(1 - x^{*2}) & -\delta c \\ \frac{\delta}{c}(2x^* + d) & 1 - \frac{\delta b}{c} \end{pmatrix},$$ (8)

and the corresponding characteristic equation can be written as

$$\lambda^2 - (2 + G\delta)\lambda + (1 + G\delta + H\delta^2) = 0,$$

where

$$G = c - cx^{*2} - \frac{b}{c}, \qquad H = bx^{*2} + 2x^* + d - b.$$

Using the corresponding discussions in [31–33], we obtain four different stability kinds of $E^*(x^*, y^*)$.

Lemma 2.2 *Let $E^*(x^*, y^*)$ be the fixed point of map (3),*
  (i) *it is a sink if one of the following conditions holds:*
      (i1) $H > 0$, $-2\sqrt{H} \le G < 0$, *and* $\delta < -\frac{G}{H}$;
      (i2) $H > 0$, $G < -2\sqrt{H}$, *and* $0 < \delta < \frac{-G - \sqrt{G^2 - 4H}}{H}$;
  (ii) *it is a source if one of the following conditions holds:*
      (ii1) $H > 0$, $-2\sqrt{H} \le G < 0$, *and* $\delta > -\frac{G}{H}$;
      (ii2) $H > 0$, $G < -2\sqrt{H}$, *and* $\delta > \frac{-G + \sqrt{G^2 - 4H}}{H}$;
      (ii3) $H > 0$ *and* $G \ge 0$;
  (iii) *it is a saddle if the following condition holds:*

$$G < -2\sqrt{H} \quad and \quad \frac{-G - \sqrt{G^2 - 4H}}{H} < \delta < \frac{-G + \sqrt{G^2 - 4H}}{H};$$

  (iv) *it is non-hyperbolic if one of the following conditions holds:*
      (iv1) $H > 0$, $G < -2\sqrt{H}$, $\delta = \frac{-G \pm \sqrt{G^2 - 4H}}{H}$, *and* $\delta \ne -\frac{2}{G}, -\frac{4}{G}$;

(iv2) $H > 0$, $-2\sqrt{H} \leq G < 0$, *and* $\delta = -\frac{G}{H}$;

(iv3) $H > 0$, $G < 0$, $\delta = -\frac{4}{G}$, *and* $G^2 = 4H$.

Only three critical cases of (iv1), (iv2), and (iv3) in Lemma 2.2 are investigated in this paper. Here, we define the following bifurcation sets F_1, F_2, and F_3:

$$F_1 = \left\{ (a,b,c,d,\delta) : \delta = \frac{-G \pm \sqrt{G^2 - 4H}}{H}, H > 0, G < -2\sqrt{H}, \delta, a, b, c, d > 0 \right\},$$

$$F_2 = \left\{ (a,b,c,d,\delta) : \delta = -\frac{G}{H}, H > 0, -2\sqrt{H} \leq G < 0, \delta, a, b, c, d > 0 \right\},$$

and

$$F_3 = \left\{ (a,b,c,d,\delta) : \delta = -\frac{4}{G}, d = \left(\frac{G}{2} + \frac{b}{c} \right)^2 - 2x^*, \delta, a, b, c, d > 0 \right\},$$

at which there exist eigenvalues with modulus 1. In this paper, we pay more attention to the local dynamics in the neighborhood of $F_{1(2,3)}$ for map (3). It is easy to find that the conditions of included in $F_{1(2,3)}$ can be satisfied at E_{11}, E_{31}, E_{32}, and E_{33}. At E_{21} and E_{22}, H may be equal to 0. In the following, bifurcation analysis is presented for E_{11}. Similar discussions can be undertaken at E_{31}, E_{32}, and E_{33}.

Let $\check{x} = x - x_{11}$ and $\check{y} = y - y_{11}$, then we transform $E_{11}(x_{11}, y_{11})$ to the origin and map (3) can be transformed as

$$\begin{pmatrix} \check{x} \\ \check{y} \end{pmatrix} \mapsto \begin{pmatrix} (1 + \delta c(1 - x_{11}{}^2))\check{x} - \delta c\check{y} - \delta c x_{11}\check{x}^2 - \frac{\delta c}{3}\check{x}^3 \\ \frac{\delta}{c}(2x_{11} + d)\check{x} + (1 - \frac{\delta b}{c})\check{y} + \frac{\delta}{c}\check{x}^2 \end{pmatrix}. \tag{9}$$

We denote the nonlinear term of map (9) as $F(X)$ ($X^T = (\check{x}, \check{y})$) and its Taylor expansion near the origin can be written as

$$F(X) = \frac{1}{2}B(X,X) + \frac{1}{6}C(X,X,X),$$

where $B(X,X)$ and $C(X,X,X)$ are multilinear functions. It follows that

$$B(x,y) = \sum_{j,k=1}^{2} \frac{\partial^2 F(\xi,\delta)}{\partial \xi_j \partial \xi_k} \Bigg|_{\xi=0} x_j y_k$$

$$= \begin{pmatrix} -2\delta c x_{11} \\ \frac{2\delta}{c} \end{pmatrix} x_1 y_1,$$

$$C(x,y,u) = \sum_{j,k,l=1}^{2} \frac{\partial^3 F(\xi,\delta)}{\partial \xi_j \partial \xi_k \partial \xi_l} \Bigg|_{\xi=0} x_j y_k u_l$$

$$= \begin{pmatrix} -2\delta c \\ 0 \end{pmatrix} x_1 y_1 u_1.$$

3 Flip bifurcation and Neimark–Sacker bifurcation

In this section, only δ is chosen as a bifurcation parameter to carry out bifurcation analysis at $E_{11}(x_{11}, y_{11})$.

When $(a, b, c, d, \delta) \in F_1$, we discuss a possible flip bifurcation at the fixed point $E_{11}(x_{11}, y_{11})$ of map (3). Here, we first require that $\delta = \frac{-G \pm \sqrt{G^2 - 4H}}{H} := \delta_1$ ($G^2 > 4H$), that is, there exists an eigenvalue $\lambda_1 = -1$. And $|\lambda_2| = |3 + G\delta_1| \neq 1$ would be satisfied if $G\delta_1 \neq -2, -4$. There exist $p, q \in \mathbb{R}^2$ such that $A(\delta_1, d, x_{11}, y_{11})q = -q$ and $A^T(\delta_1, d, x_{11}, y_{11})p = -p$. After calculation, p, q can be chosen as

$$q \sim \left(-2 + \frac{\delta_1 b}{c}, \frac{\delta_1}{c}(2x_{11} + d) \right)^T,$$

$$p \sim \left(-2 + \frac{\delta_1 b}{c}, -\delta_1 c \right)^T.$$

After normalizing p with respect to q, we have

$$q = \left(-2 + \frac{\delta_1 b}{c}, \frac{\delta_1}{c}(2x_{11} + d) \right)^T,$$

$$p = \gamma \left(-2 + \frac{\delta_1 b}{c}, -\delta_1 c \right)^T,$$

where

$$\frac{1}{\gamma} = \left(2 - \frac{\delta_1 b}{c} \right)^2 - \delta_1{}^2 (2x_{11} + d).$$

After a series of transformations similarly introduced in [34], we transform map (9) to the following normal form on the center manifold at $\delta = \delta_1$:

$$\xi \mapsto -\xi + \widetilde{c}(\delta_1)\xi^3 + O(\xi^4),$$

where

$$\widetilde{c}(\delta_1) = \frac{1}{6}\langle p, C(q, q, q) \rangle - \frac{1}{2}\langle p, B(q, (A(\delta_1) - I_2)^{-1} B(q, q)) \rangle,$$
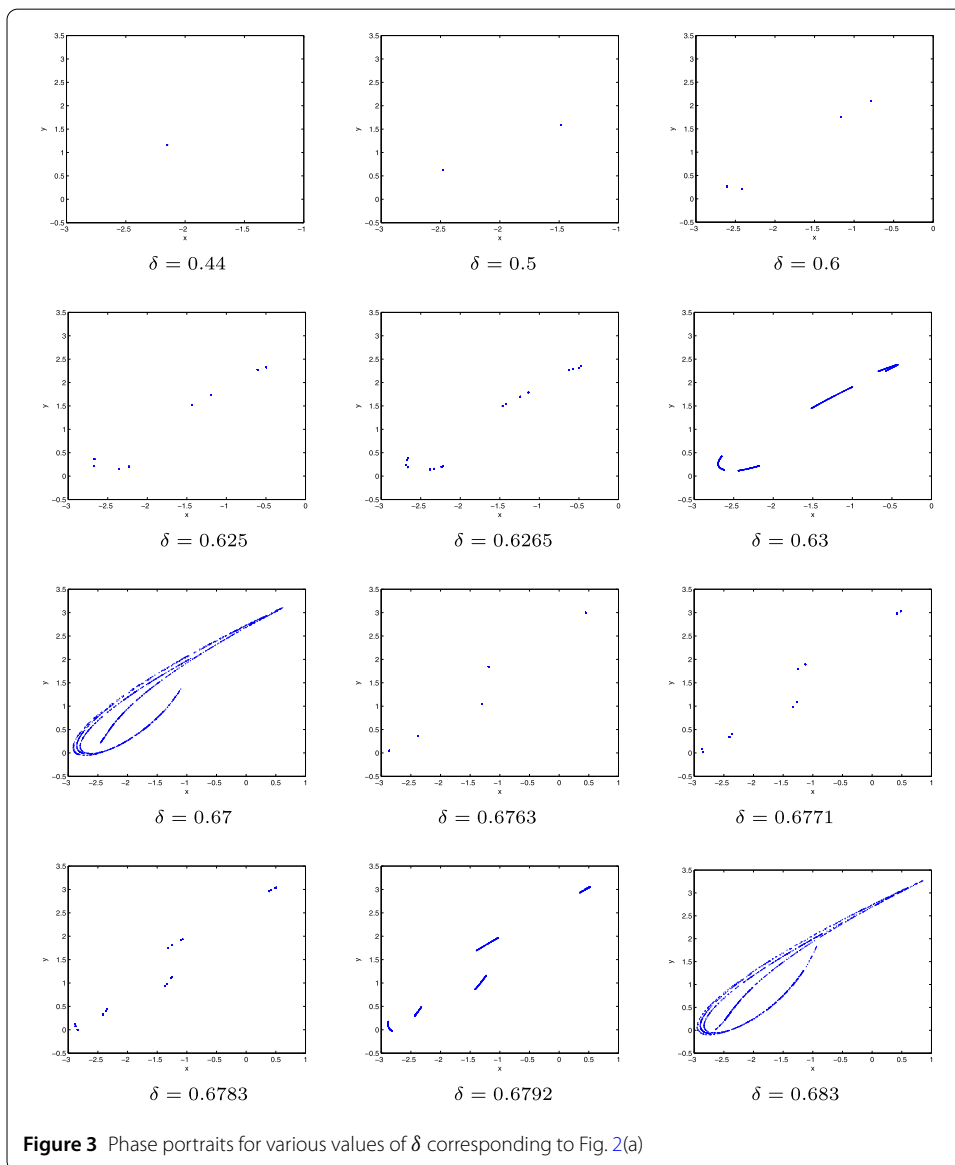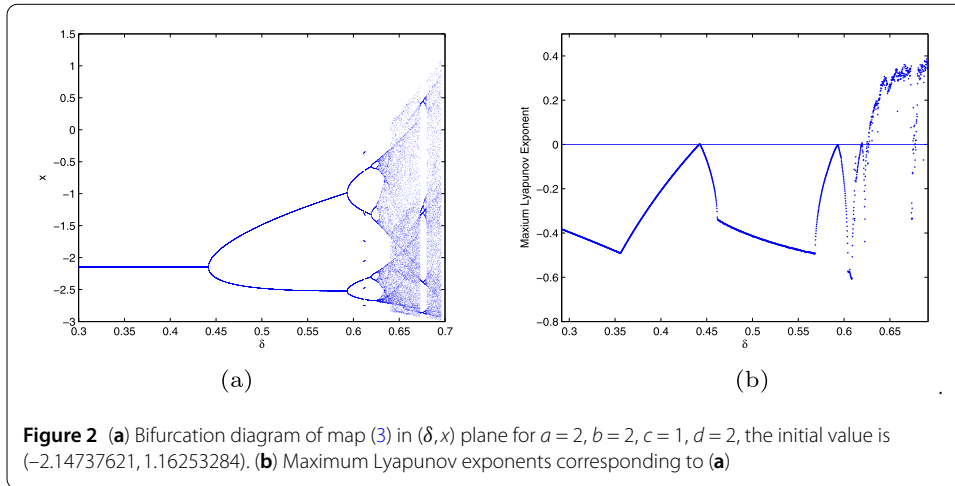
which determines the stability of the newborn period-doubling orbits and I_2 is a 2×2 identity matrix.

Using the corresponding theorems in [34–38], we obtain the following conclusions.

Theorem 3.1 *If $G^2 > 4H$, $G\delta_1 \neq -2, -4$, and $\widetilde{c}(\delta_1) \neq 0$, then a flip bifurcation occurs at $E_{11}(x_{11}, y_{11})$ of map (3) when $\delta = \delta_1$. Further, if $\widetilde{c}(\delta_1) < 0$ (resp., $\widetilde{c}(\delta_1) > 0$), then the bifurcation is subcritical (resp., supercritical), that is, the newborn period-two cycles are stable (resp., unstable).*

In Sect. 5, some parameter values will be chosen from F_1 to show the cascade of period-doubling. The stability of fixed point changes and orbits with different periods emerge as δ varies (see Figs. 2–3).

Next, the Neimark–Sacker bifurcation of map (3) at $E_{11}(x_{11}, y_{11})$ is discussed if $H > 0$, $-2\sqrt{H} \leq G < 0$, and $\delta_2 = -\frac{G}{H}$.

Figure 2 (**a**) Bifurcation diagram of map (3) in (δ, x) plane for $a = 2$, $b = 2$, $c = 1$, $d = 2$, the initial value is $(-2.14737621, 1.16253284)$. (**b**) Maximum Lyapunov exponents corresponding to (**a**)

Figure 3 Phase portraits for various values of δ corresponding to Fig. 2(a)

To investigate the local dynamics near the origin of map (3), we construct the following characteristic equation:

$$\lambda^2 + p(\delta)\lambda + q(\delta) = 0,$$

where

$$p(\delta) = -2 - G\delta,$$

$$q(\delta) = 1 + G\delta + H\delta^2.$$

Then

$$\left|\lambda(\delta)\right| = \sqrt{q(\delta)}, \qquad l = \frac{d|\lambda|}{d\delta}\bigg|_{\delta=\delta_2} = -\frac{G}{2} > 0.$$

In addition, $|\lambda(\delta_2)| = 1$ and we need $p(\delta_2) \neq 0, 1$, that means

$$G\delta_2 \neq -2, -3,$$

then $\lambda^n(\delta_2) \neq 1$, $n = 1, 2, 3, 4$. Here, $A(\delta_2)$ is used as the short form of $A(\delta_2, d, x_{11}, y_{11})$. Let $p, q \in \mathbb{C}^2$ such that

$$A(\delta_2)q = \lambda(\delta_2)q, \qquad A(\delta_2)\bar{q} = \overline{\lambda(\delta_2)}\bar{q},$$

and

$$A^T(\delta_2)p = \overline{\lambda(\delta_2)}p, \qquad A^T(\delta_2)\bar{p} = \lambda(\delta_2)\bar{p}.$$

It is easy to get

$$q \sim \left(1 + \frac{\delta_2 b}{c} - \lambda(\delta_2), -\delta_2(2x_{11} + d)\right)^T,$$

$$p \sim \left(1 + \frac{\delta_2 b}{c} - \overline{\lambda(\delta_2)}, -\delta_2 c\right)^T.$$

After normalizing, we have

$$q = \left(1 + \frac{\delta_2 b}{c} - \lambda(\delta_2), -\delta_2(2x_{11} + d)\right)^T,$$

$$p = \check{\gamma}\left(1 + \frac{\delta_2 b}{c} - \overline{\lambda(\delta_2)}, -\delta_2 c\right)^T,$$

where

$$\frac{1}{\check{\gamma}} = \left(1 + \frac{\delta_2 b}{c} - \overline{\lambda(\delta_2)}\right)^2 + \delta_2^2 c(2x_{11} + d).$$

After a series of transformations similarly introduced in [34], we can transform map (9) to the normal form on the center manifold at $\delta = \delta_2$ as follows:

$$z \mapsto e^{i\theta(\delta_2)} z \big(1 + d_1 |z|^2\big) + O\big(|z|^4\big),$$

where $e^{i\theta(\delta_2)} = \lambda(\delta_2)$, $z \in \mathbb{Z}^2$ and the real number $\widetilde{d}(\delta_2) = \operatorname{Re} d_1$ is given by the following formula:

$$
\begin{aligned}
\widetilde{d}(\delta_2) = \frac{1}{2} \operatorname{Re} \big\{ e^{-i\theta(\delta_2)} \big[\langle p, C(q,q,\bar{q}) \rangle + 2\langle p, B\big(q, \big(I_2 - A(\delta_2)\big)^{-1} B(q,\bar{q})\big) \rangle \\
+ \langle p, B\big(\bar{q}, \big(e^{2i\theta(\delta_2)} I_2 - A(\delta_2)\big)^{-1} B(q,q)\big) \rangle \big] \big\},
\end{aligned}
$$

which determines whether the bifurcating closed invariant curve is attracting or repelling.

Using the corresponding theorems in [34–38], we obtain the following conclusions.

Theorem 3.2 *If the conditions $G\delta_2 \neq -2, -3$ hold and $\widetilde{d}(\delta_2) \neq 0$, then a Neimark–Sacker bifurcation occurs at $E_{11}(x_{11}, y_{11})$ of map* (3) *when $\delta = \delta_2$. Further, the sign of $\widetilde{d}(\delta_2)$ decides the stability of a bifurcating closed invariant curve. If $\widetilde{d}(\delta_2) < 0$ (resp., > 0), then the bifurcating closed invariant curve is attracting (resp., repelling) for $\delta > \delta_2$ (resp., $< \delta_2$).*

In Sect. 5, parameters $(a, b, c, d, \delta_2) \in F_2$ are chosen to illustrate the way of how a fixed point changes to a closed invariant curve through Neimark–Sacker bifurcation for map (3) in Figs. 4–5.

4 Bifurcation with 1 : 2 resonance

In this section, δ and d are chosen as free parameters to carry out bifurcation analysis at 1 : 2 resonance point. Note that the Jacobian matrix for $(a, b, c, d, \delta) = (a, b, c, d^*, \delta^*) \in F_3$ at $E_{11}(x_{11}, y_{11})$ is

$$
A\big(\delta^*, d^*, x_{11}, y_{11}\big) =
\begin{pmatrix}
-3 - \frac{4b}{Gc} & \frac{4c}{G} \\
-\frac{4}{Gc}\big(\frac{G}{2} + \frac{b}{c}\big)^2 & 1 + \frac{4b}{Gc}
\end{pmatrix}
=: A\big(\delta^*, d^*\big).
$$

We can always select two linearly independent eigenvectors $p_i \in \mathbb{R}^2$ of $A(\delta^*, d^*)$ such that

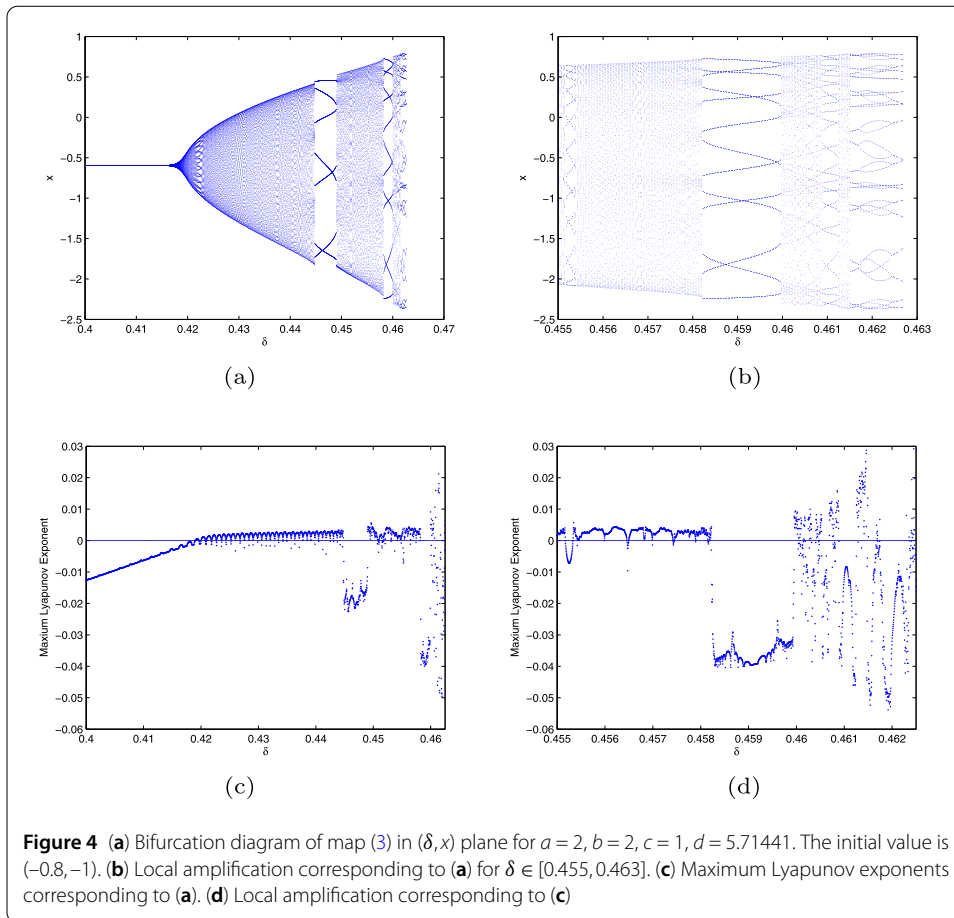$$A\big(\delta^*, d^*\big) p_1 = -p_1, \qquad A\big(\delta^*, d^*\big) p_2 = -p_2 + p_1,$$

and similarly adjoint eigenvectors $q_i \in \mathbb{R}^2$ of the transposed matrix of $A^T(\delta^*, d^*)$

$$A^T\big(\delta^*, d^*\big) q_1 = -q_1, \qquad A^T\big(\delta^*, d^*\big) q_2 = -q_2 + q_1,$$

so that $\langle p_1, q_2 \rangle = \langle p_2, q_1 \rangle = 1$ and $\langle p_1, q_1 \rangle = \langle p_2, q_2 \rangle = 0$.

Herein, the following eigenvectors are chosen to transform map (9) to the 1 : 2 resonance normal form at $(\delta, d) = (\delta^*, d^*)$:

$$
p_1 =
\begin{pmatrix}
\frac{2c^2}{Gc+2b} \\
1
\end{pmatrix}, \qquad
p_2 =
\begin{pmatrix}
-\frac{Gc^3}{(Gc+2b)^2} \\
0
\end{pmatrix},
$$

Figure 4 (**a**) Bifurcation diagram of map (3) in (δ, x) plane for $a = 2$, $b = 2$, $c = 1$, $d = 5.71441$. The initial value is $(-0.8, -1)$. (**b**) Local amplification corresponding to (**a**) for $\delta \in [0.455, 0.463]$. (**c**) Maximum Lyapunov exponents corresponding to (**a**). (**d**) Local amplification corresponding to (**c**)

$$
q_1 = \begin{pmatrix} -\frac{Gc+2b}{2c^2} \\ 1 \end{pmatrix}, \qquad q_2 = \begin{pmatrix} 0 \\ \frac{Gc+2b}{2c^2} \end{pmatrix}.
$$

After a series of transformations which can be constructed similar to those in [34], we can transform map (9) to the following normal form at $(\delta, d) = (\delta^*, d^*)$:
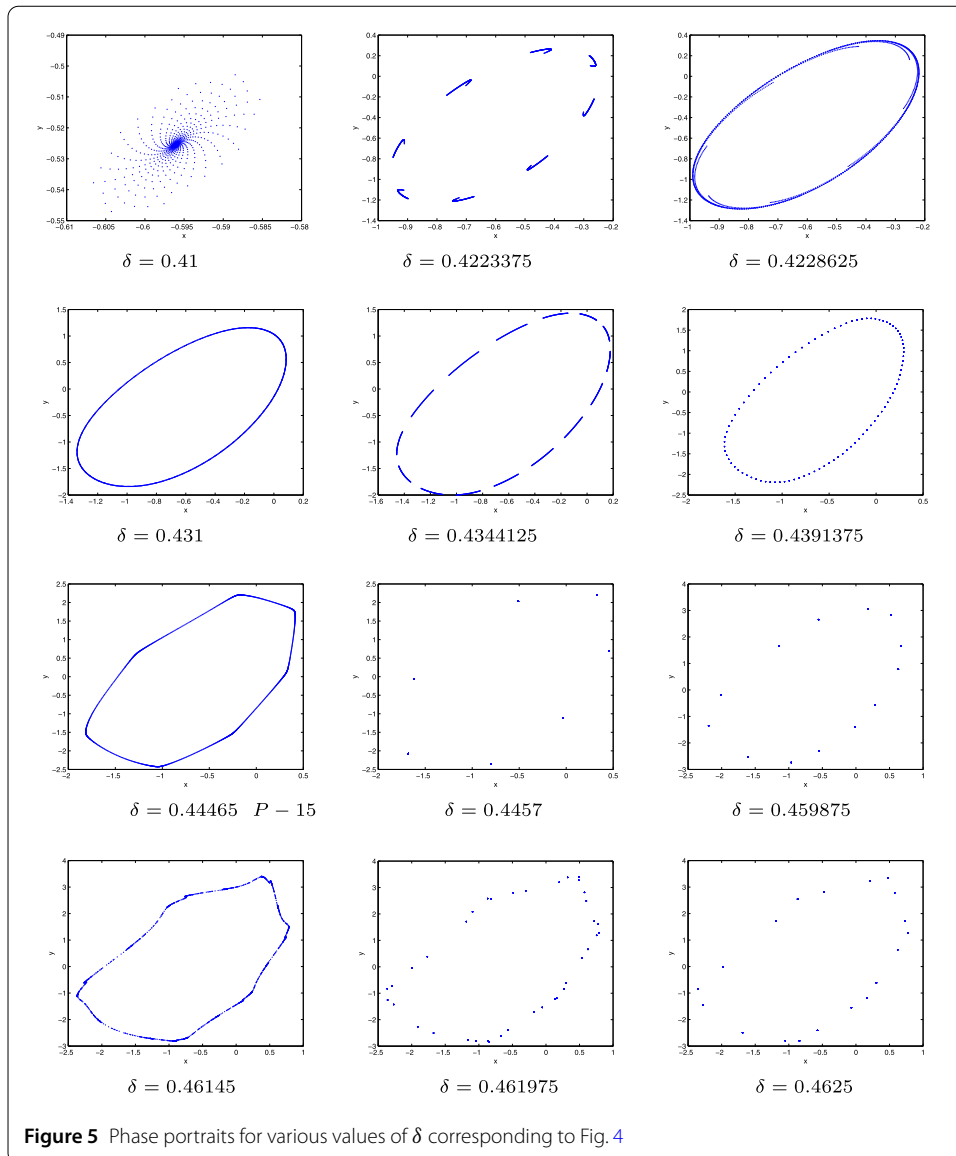
$$
\begin{pmatrix} \xi_1 \\ \xi_2 \end{pmatrix} \mapsto \begin{pmatrix} -1 & 1 \\ \beta_1 & -1 + \beta_2 \end{pmatrix} \begin{pmatrix} \xi_1 \\ \xi_2 \end{pmatrix} + \begin{pmatrix} 0 \\ \widetilde{C}(\beta)\xi_1^3 + \widetilde{D}(\beta)\xi_1^2\xi_2^1 \end{pmatrix} + O\big(|z|^4\big),
$$

where $\beta = (\beta_1, \beta_2)^T$, $\beta_{1(2)} = \beta_{1(2)}(\delta, d)$, which can be defined as follows:

$$
\beta_1(\delta, d) = b_{10}(\delta, d) + a_{01}(\delta, d)b_{10}(\delta, d) - a_{10}(\delta, d)b_{01}(\delta, d),
$$

$$
\beta_2(\delta, d) = a_{10}(\delta, d) + b_{01}(\delta, d)
$$

and

$$
a_{01}(\delta, d) = \big\langle q_2, \big[A(\delta, d) - A\big(\delta^*, d^*\big)\big], p_1\big\rangle, \qquad a_{10}(\delta, d) = \big\langle q_2, \big[A(\delta, d) - A\big(\delta^*, d^*\big)\big], p_2\big\rangle,
$$

$$
b_{01}(\delta, d) = \big\langle q_1, \big[A(\delta, d) - A\big(\delta^*, d^*\big)\big], p_1\big\rangle, \qquad b_{10}(\delta, d) = \big\langle q_1, \big[A(\delta, d) - A\big(\delta^*, d^*\big)\big], p_2\big\rangle.
$$

Figure 5 Phase portraits for various values of δ corresponding to Fig. 4

Using the algorithms constructed in [34], we get the two critical normal form coefficients

$$C_1\big(\beta\big(\delta^*,d^*\big)\big) = 4\widetilde{C}\big(\beta\big(\delta^*,d^*\big)\big)$$

and

$$D_1\big(\beta\big(\delta^*,d^*\big)\big) = -2\widetilde{D}\big(\beta\big(\delta^*,d^*\big)\big) - 6\widetilde{C}\big(\beta\big(\delta^*,d^*\big)\big);$$

$$\widetilde{C}\big(\beta\big(\delta^*,d^*\big)\big) = \frac{1}{6}\big\langle p_1, C(q_0,q_0,q_0) + 3B\big(q_0,\big(I_2 - A\big(\delta^*,d^*\big)\big)^{-1}B(q_0,q_0)\big)\big\rangle,$$

and

$$\widetilde{D}\big(\beta\big(\delta^*,d^*\big)\big) = \frac{1}{2}\big[\big\langle p_1, 2B(q_0,h_{11}) + B(q_1,h_{20}) + C(q_0,q_0,q_1)\big\rangle$$
$$+ \big\langle p_0, 3B(q_0,h_{20}) + C(q_0,q_0,q_0)\big\rangle\big],$$

which determines the direction of bifurcation of a closed invariant curve and

$$h_{20} = -\big(A\big(\delta^*, d^*\big) - I_2\big)^{-1} B(q_0, q_0),$$

$$h_{11} = -\big(A\big(\delta^*, d^*\big) - I_2\big)^{-1}\big[B(q_0, q_1) - \big(A\big(\delta^*, d^*\big) - I_2\big)^{-1} B(q_0, q_0)\big].$$

From the related theorems in [34, 36], we obtain three kinds of one-parameter bifurcations emanated from the origin of map (9) and compute the representation for δ^* and d^*.

Theorem 4.1 *If $C_1(\delta^*, d^*) \neq 0$ and $D_1(\delta^*, d^*) \neq 0$, then there exist three different kinds of bifurcation curves for map* (3):

(a) *Pitchfork bifurcation occurs on the curve $PF = \{(\beta_1, \beta_2) : \beta_1 = 0\}$;*

(b) *Neimark–Sacker bifurcation occurs on the curve*
   $H = \{(\beta_1, \beta_2) : \beta_1 = -\beta_2 + O(|\beta_1| + |\beta_2|)^2, \beta_1 < 0\}$;

(c) *Heteroclinic bifurcation occurs on the curve*
   $HL = \{(\beta_1, \beta_2) : \beta_1 = -\frac{5}{3}\beta_2 + O(|\beta_1| + |\beta_2|)^2, \beta_1 < 0\}$.

In Sect. 5 we will choose $(a, b, c, d, \delta) \in F_3$ to illustrate the dynamics in the neighborhood of 1 : 2 resonance point, which implies that there exist a flip bifurcation curve and a Neimark–Sacker bifurcation curve which intersect at 1 : 2 resonance point.

5 Numerical analysis

In this section, numerical analysis is carried out with MATLAB to illustrate the qualitative behaviors described in the above lemmas and theorems for map (3).

When $a = 2$, $b = 2$, $c = 1$, and $d = 2$, there are $D = 1 > 0$ and $F(-1)F(0) = \frac{14}{3} > 0$. From the second case of Lemma 2.1, there exists a unique fixed point $(-2.149376214918635, 1.161532841710343)$ for map (3). When $\delta = \delta_1$, the flip bifurcation occurs at $(-2.149376214918635, 1.161532841710343)$ with $\widetilde{c}(\delta_1) = -0.5451227$. As δ increases, then the fixed point $(-2.149376214918635, 1.161532841710343)$ of map (3) will lose its stability, two fixed points could bifurcate from it, and eventually period-doubling phenomena occur. Bifurcation diagrams presented in Fig. 2(a) show us the bifurcating process and the cascade of period-doubling emerges for some values of δ. For clarity, some typical phase portraits are plotted in Fig. 3. For $\delta \in (0.5, 0.6783)$, we observe period-$2n$, $5n$ ($n = 1, 2, 4$) orbits. When $\delta = 0.67$, the chaotic phenomena occur. In Fig. 2(b) we calculated maximum Lyapunov exponents to illustrate the stability of the fixed points. When δ lies in a small neighborhood of 0.67, the corresponding exponents are positive, which implies the occurrence of the chaotic phenomena [39, 40].

When $a = 2$, $b = 2$, $c = 1$, $d = 5.71441$, there is $D = -6.42882 < 0$. From the first case of Lemma 2.1, we obtain a unique fixed point $(-0.596089234530279, -0.525487953584638)$ for map (3). When $\delta \approx 0.41923114$, the Neimark–Sacker bifurcation emerges from $(-0.596089234530279, -0.525487953584638)$ and its eigenvalues are $\lambda_{1,2} \approx 0.715903334775152 \pm 0.698199409379453i$. For $\delta = 0.41923114$, there are $|\lambda| = 1$, $l = \frac{d|\lambda|}{d\delta} = 0.677661187761447 > 0$, and $\widetilde{d}(\delta_2) = -0.01226361 < 0$. It provides a case study for Theorem 3.2.

Bifurcation diagrams presented in Figs. 4(a) and (b) show us the bifurcating process and the emergence of a closed invariant curve. As the parameter δ varies, the stability of the

fixed point changes and is eventually enclosed by a closed invariant curve. From Figs. 4(b), there exist "period bubbling" phenomena when $\delta \in (0.4615, 0.4625)$ [41].

As in the flip bifurcation case, the maximum Lyapunov exponents were also computed and plotted in Figs. 4(c) and (d) that show the occurrence of periodic orbits, critical bifurcation sets, and chaotic region as δ varies.
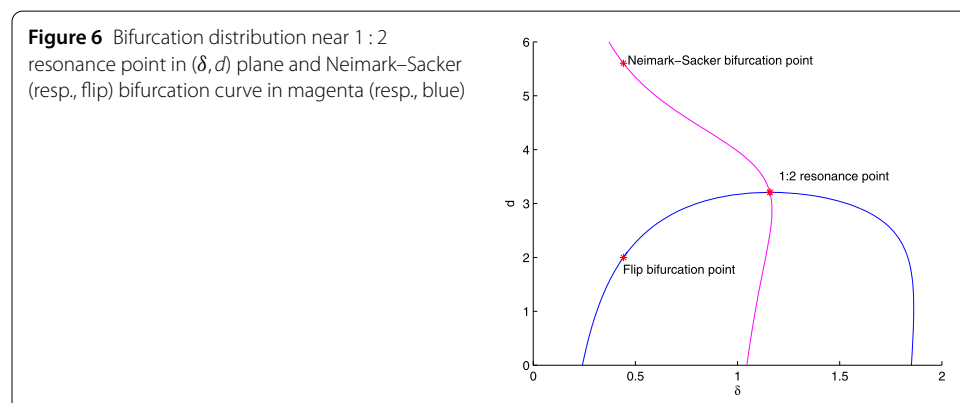
The selected phase portraits are disposed, they illustrate the process of the Neimark–Sacker bifurcation, that is, a unique closed invariant curve bifurcates from the stable fixed point $(-0.596089234530279, -0.525487953584638)$ and encloses it in Fig. 5. When $\delta = 0.4457$, the closed invariant curve changes to a period-7 orbit, and "period bubbling" phenomena occur. From Fig. 5 we see that there exist period-$7n$, $19n$ ($n = 1, 2$) orbits, quasi-period orbits, and chaotic sets.
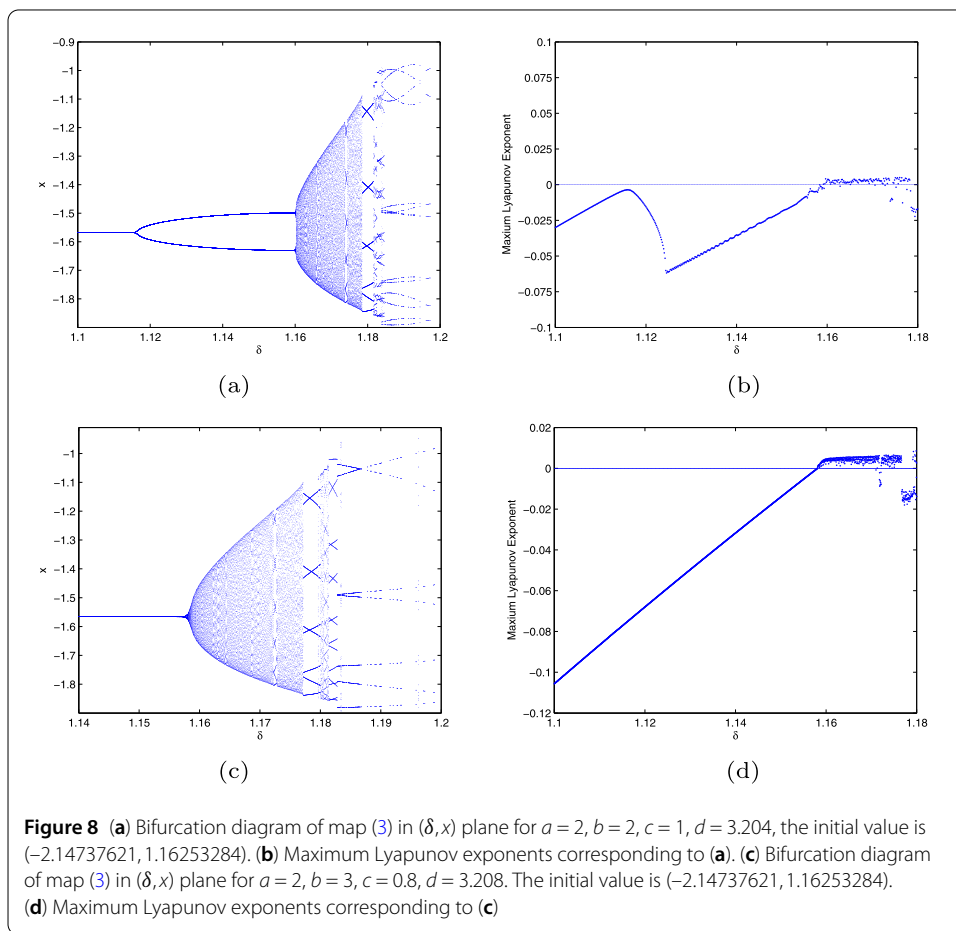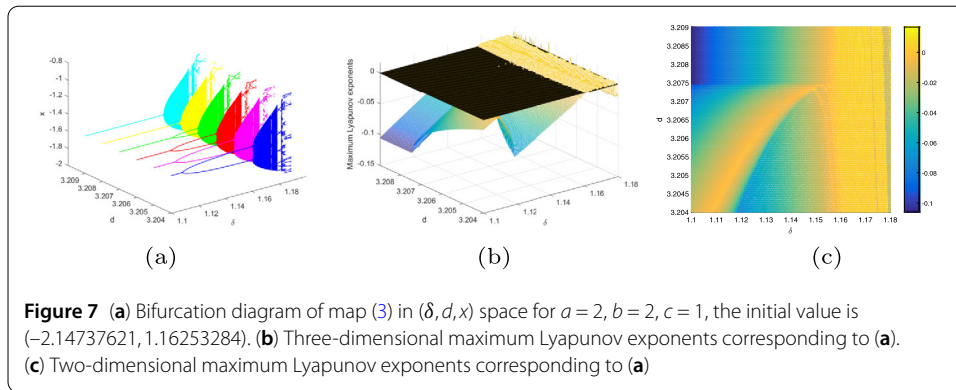
When $a = 2$, $b = 2$, $c = 1$, $d = 3.20745$, there is $D = -1.4149 < 0$. From the first case of Lemma 2.1, we get a unique fixed point $(-1.5664125, -0.28527086)$ for map (3). After computation, we obtain that the eigenvalues of $A(\delta^*, d^*, -1.5664125, -0.28527086)$ are $\lambda_{1,2} = -1$ when $\delta^* = 1.1581956$ and $d^* = 3.20745$ with $C_1 = -4.540894 \neq 0$ and $D_1 = -4.028139 \neq 0$. The fixed point $(-1.5664125, -0.28527086)$ is a $1 : 2$ resonance point from Theorem 4.1. Furthermore, the condition $C_1 = -4.540894 < 0$ implies that there exists a period-2 closed invariant curve bifurcating from fixed points of map (3). Since C_1 and D_1 are negative, the bifurcation pictures in the small neighborhood of $(-1.5664125, -0.28527086)$ are qualitatively the same as Fig. 9.10 given in Chap. 9 of [34].

Bifurcation continuations of $1 : 2$ resonance point are carried out by using MatcontM, and bifurcation distribution near the resonance point is plotted in Fig. 6. From Fig. 6, a flip curve and a Neimark–Sacker curve are plotted in different colors and intersect at $1 : 2$ resonance point.

When $a = 2$, $b = 2$, $c = 1$, and δ, d vary near $(1.1581956, 3.20745)$, three-dimensional bifurcation diagrams for map (3) are presented in Fig. 7(a). The corresponding maximum Lyapunov exponents are calculated and disposed in Fig. 7(b), especially the three-dimensional figure is projected on the parametric plane, see Fig. 7(c), to show the occurrence of the chaos and periodic oscillations near the fixed point $(-1.5664125, -0.28527086)$ clearly. Related phase portraits are plotted in Fig. 9, too.

To further illustrate the local dynamics of a $1 : 2$ resonance point, we consider the following cases. When $a = 2$, $b = 2$, $c = 1$, $d = 3.204$, and $1.1 \leq \delta < 1.8$, there exist pitchfork bifurcation phenomena near $(-1.5664125, -0.28527086)$ for map (3). Bifurcation diagrams and the corresponding maximum Lyapunov exponents are calculated and plotted

Figure 6 Bifurcation distribution near 1 : 2 resonance point in (δ, d) plane and Neimark–Sacker (resp., flip) bifurcation curve in magenta (resp., blue)

Figure 7 (**a**) Bifurcation diagram of map (3) in (δ, d, x) space for $a = 2$, $b = 2$, $c = 1$, the initial value is $(-2.14737621, 1.16253284)$. (**b**) Three-dimensional maximum Lyapunov exponents corresponding to (**a**). (**c**) Two-dimensional maximum Lyapunov exponents corresponding to (**a**)

Figure 8 (**a**) Bifurcation diagram of map (3) in (δ, x) plane for $a = 2$, $b = 2$, $c = 1$, $d = 3.204$, the initial value is $(-2.14737621, 1.16253284)$. (**b**) Maximum Lyapunov exponents corresponding to (**a**). (**c**) Bifurcation diagram of map (3) in (δ, x) plane for $a = 2$, $b = 3$, $c = 0.8$, $d = 3.208$. The initial value is $(-2.14737621, 1.16253284)$. (**d**) Maximum Lyapunov exponents corresponding to (**c**)

in Figs. 8(a)–(b). Related phase portraits are plotted in Fig. 9. When $a = 2$, $b = 2$, $c = 1$, $d = 3.208$, and $1.1 \leq \delta < 1.8$, there exist Neimark–Sacker bifurcation phenomena near $(-1.565598214673778, -0.286453450549223)$ for map (3). Bifurcation diagrams and the corresponding maximum Lyapunov exponents are calculated and plotted in Figs. 8(c)–(d).

Figure 9 shows the phase portraits of map (3) corresponding to Figs. 7–8. From Fig. 9, we can see that the fixed point $(-1.5664125, -0.28527086)$ becomes two fixed points through pitchfork bifurcation, and these two fixed points change to two stable closed invariant

Figure 9 Phase portraits for various values of (δ, d) corresponding to Figs. 7–8
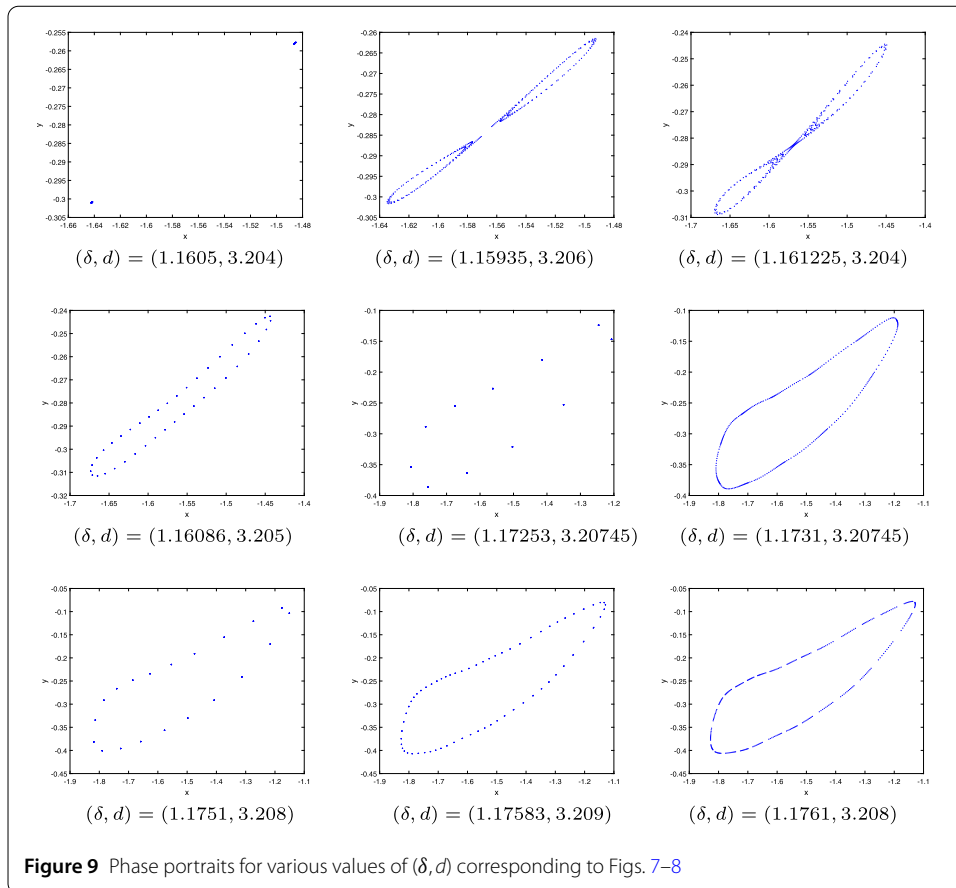
curves. Furthermore, as the parameters (δ, d) vary, the distance between them becomes smaller and smaller, merges into one stable invariant curve, and eventually leads to chaos.

6 Conclusion

In this paper, we explored three kinds of bifurcations at the fixed points of map (3) and showed that the discrete model could undergo two kinds of one-parameter bifurcations and 1 : 2 resonance which includes a pitchfork bifurcation, a Neimark–Sacker bifurcation, and a heteroclinic bifurcation. Moreover, the conditions of two kinds of one-parameter bifurcations are derived by using the inner product method and normal form method. We computed the sufficient conditions for the occurrence of 1 : 2 resonance and provided the representation for a pitchfork bifurcation curve, a Neimark–Sacker bifurcation curve, and a heteroclinic bifurcation curve. From the presented phase portraits, periodic orbits, quasi-periodic orbits, and chaotic phenomena emerge, which implies that the state variables x and y can coexist in the stable periodic orbits and invariant curve or behave chaotic. These show that more complex dynamics, such as much richer orbits of different patterns, are observed than in the continuous version.

Especially, as the generate case of flip and Neimark–Sacker bifurcation, we pay more attention to the 1 : 2 resonance. When the 1 : 2 resonance of a dynamical system occurs, there exists at least a heteroclinic orbit which arises from invariant curves with double period in the phase space, see Fig. 9. As one of global bifurcations, the occurrence of heteroclinic bifurcation implies that interactions between different activities would be more

complex. Here, only the sufficient conditions of a heteroclinic bifurcation are computed, and we leave further analysis for future work. Phase portraits show us some symmetric phenomena, in fact the normal form of $1 : 2$ resonance is $\mathbb{Z}_2$ symmetric, that is, the map is invariant under the rotation P ($P^2 = I_2$) through the angle π.

Availability of data and materials
Not applicable.

Competing interests
The authors declare that they have no competing interests.

Authors' contributions
All authors contributed equally in this article. All authors read and approved the final manuscript.

Authors' information
Not applicable.

Publisher's Note
Springer Nature remains neutral with regard to jurisdictional claims in published maps and institutional affiliations.

References
1. Hodgkin, A.L., Huxley, A.F.: A qualitative description of membrane current and its application to conduction and excitation in nerve. J. Physiol. **117**, 500–544 (1952)
2. FitzHugh, R.: Impulses and physiological state in theoretical models of nerve membrane. Biophys. J. **1**(6), 445–467 (1961)
3. Nagumo, J., Arimoto, S., Yoshizawa, S.: An active pulse transmission line simulating nerve axon. Proc. IRE **50**(10), 2061–2070 (1962)
4. Hindmarsh, J.L., Rose, R.M.: A model of the nerve impulse using two first-order differential equations. Nature **296**, 162–164 (1982)
5. Hindmarsh, J.L., Rose, R.M.: A model of neuronal bursting using three coupled first order differential equations. Proc. R. Soc. Lond. B **221**, 87–102 (1984)
6. Zhang, D.G., Zhang, Q., Zhu, X.Y.: Exploring a type of central pattern generator based on Hindmarsh–Rose model: from theory to application. Int. J. Neural Syst. **25**(1), 1450028 (2015)
7. Simo Domguia, U., Abodba, L.T., Woafo, P.: Dynamical behavior of a capacitive microelectromechanical system powered by a Hindmarsh–Rose electronic oscillator. J. Comput. Nonlinear Dyn. **11**(5), 051006 (2016)
8. Wu, K.J., Luo, T.Q., Lu, H.W., Wang, Y.: Bifurcation study of neuron firing activity of the modified Hindmarsh–Rose model. Neural Comput. Appl. **27**(3), 739–747 (2016)
9. Yu, Y., Cao, H.J.: Integral step size makes a difference to bifurcations of a discrete-time Hindmarsh–Rose model. Int. J. Bifurc. Chaos **25**(2), 1550029 (2015)
10. Barrio, R., Ibáñez, S., Pérez, L.: Hindmarsh–Rose model: close and far to the singular limit. Phys. Lett. A **381**(6), 597–603 (2017)
11. Buzzi, C., Llibre, J., Medrado, J.: Hopf and zero-Hopf bifurcations in the Hindmarsh–Rose system. Nonlinear Dyn. **83**(3), 1549–1556 (2016)
12. Dtchetgnia Djeundam, S.R., Yamapi, R., Filatrella, G., Kofane, T.C.: Stability of the synchronized network of Hindmarsh–Rose neuronal models with nearest and global couplings. Commun. Nonlinear Sci. Numer. Simul. **22**(1–3), 545–563 (2015)
13. Li, B., He, Z.M.: Bifurcations and chaos in a two-dimensional discrete Hindmarsh–Rose model. Nonlinear Dyn. **76**(1), 697–715 (2014)
14. Li, B., He, Z.M.: 1 : 3 resonance and chaos in a two-dimensional discrete Hindmarsh–Rose model. J. Appl. Math. **2014**, Article ID 896478 (2014)
15. Li, B., He, Z.M.: 1 : 2 and 1 : 4 resonances in a two-dimensional discrete Hindmarsh–Rose model. Nonlinear Dyn. **79**(1), 705–720 (2015)
16. Liu, X.L., Liu, S.Q.: Codimension-two bifurcations analysis in two-dimensional Hindmarsh–Rose model. Nonlinear Dyn. **67**(1), 847–857 (2012)
17. Rech, P.C.: Dynamics of a neuron model in different two-dimensional parameter-spaces. Phys. Lett. A **375**(12), 1461–1464 (2011)
18. Felicio, C.C., Rech, P.C.: Arnold tongues and the devil's staircase in a discrete-time Hindmarsh–Rose neuron model. Phys. Lett. A **379**(43–44), 2845–2847 (2015)

19. Da Silva, A., Rech, P.C.: Chaos and periodicity in a discrete-time Baier–Sahle model. Asian J. Math. Comput. Res. **15**(2), 123–130 (2017)
20. Rech, P.C.: Organization of the periodicity in the parameter-space of a glycolysis discrete-time mathematical model. J. Math. Chem. **57**(2), 632–637 (2019). https://doi.org/10.1007/s10910-018-0976-4
21. Chen, Q.L., Teng, Z.D.: Codimension-two bifurcation analysis of a discrete predator–prey model with nonmonotonic functional response. J. Differ. Equ. Appl. **23**(12), 2093–2115 (2017)
22. Govaerts, W., Khoshsiar Ghaziani, R., Kuznetsov, Y.A., Meijer, H.G.E.: Numerical methods for two-parameter local bifurcation analysis of maps. SIAM J. Sci. Comput. **29**(6), 2644–2667 (2007)
23. Huang, J.C., Liu, S.H., Ruan, S.G., Xiao, D.M.: Bifurcations in a discrete predator–prey model with nonmonotonic functional response. J. Math. Anal. Appl. **464**, 201–230 (2018)
24. Ren, J.L., Yu, L.P.: Codimension-two bifurcation, chaos and control in a discrete-time information diffusion model. J. Nonlinear Sci. **26**(6), 1895–1931 (2016)
25. Ren, J.L., Yu, L.P., Zhu, H.P.: Dynamic analysis of discrete-time, continuous-time and delayed feedback jerky equations. Nonlinear Dyn. **86**(1), 107–130 (2016)
26. Yi, N., Zhang, Q., Liu, P., Lin, Y.: Codimension-two bifurcations analysis and tracking control on a discrete epidemic model. J. Syst. Sci. Complex. **24**(1), 1033–1056 (2011)
27. Yue, D.D., Guan, Z.H., Chen, J., Ling, G., Wu, Y.H.: Bifurcations and chaos of a discrete-time in genetic regulatory networks. Nonlinear Dyn. **87**, 567–586 (2017)
28. Tsuji, S., Ueta, T., Kawakami, H., Fujii, H., Aihara, K.: Bifurcations in two-dimensional Hindmarsh–Rose type model. Int. J. Bifurc. Chaos **17**(3), 985–998 (2007)
29. Chen, S.S., Cheng, C.Y., Lin, Y.R.: Application of in two-dimensional Hindmarsh–Rose type model for bifurcation analysis. Int. J. Bifurc. Chaos **23**(3), 1350055 (2013)
30. Heidarpur, M., Ahmadi, A., Kandalaft, N.: A digital implementation of 2D Hindmarsh–Rose neuron. Nonlinear Dyn. **89**(3), 2257–2272 (2017)
31. He, Z.M., Lai, X.: Bifurcations and chaotic behavior of a discrete-time predator–prey system. Nonlinear Anal., Real World Appl. **12**(1), 403–417 (2011)
32. Jiang, X.W., Ding, L., Guan, Z.H., Yuan, F.S.: Bifurcation and chaotic behavior of a discrete-time Ricardo–Malthus model. Nonlinear Dyn. **71**(3), 437–446 (2013)
33. Liu, X.L., Xiao, D.M.: Complex dynamic behaviors of a discrete-time predator–prey system. Chaos Solitons Fractals **32**(1), 80–94 (2007)
34. Kuznetsov, Y.A.: Elements of Applied Bifurcation Theory, 3rd edn. Springer, New York (2004)
35. Carr, J.: Application of Center Manifold Theory. Springer, New York (1981)
36. Guckenheimer, J., Holmes, P.: Nonlinear Oscillations, Dynamical Systems, and Bifurcations of Vector Fields. Springer, Berlin (1983)
37. Robinson, C.: Dynamical Systems: Stability, Symbolic Dynamics and Chaos, 2nd edn. CRC Press, Boca Raton (1999)
38. Wiggins, S.: Introduction to Applied Nonlinear Dynamical Systems and Chaos. Springer, New York (2003)
39. Alligood, K.T., Sauer, T.D., Yorke, J.A.: Chaos—An Introduction to Dynamical Systems. Springer, New York (1996)
40. Ott, E.: Chaos in Dynamical Systems, 2nd edn. Cambridge University Press, Cambridge (2002)
41. Vandermeer, J.: Period 'bubbling' in simple ecological models: pattern and chaos formation in a quartic model. Ecol. Model. **95**(2–3), 311–317 (1997)